Mathematical Modelling of Weld Phenomena 9
Published by Technische Universitat GRAZ, eds H. Cerjak and N. Enzinger, 2010, 239-252

MODELLING OF RESIDUAL STRESS MINIMIZATION THROUGH MARTENSITIC TRANSFORMATION IN STAINLESS STEEL WELDS

H. DAI*, A.F. MARK*, R. MOAT*, A.A. SHIRZADI**, H.K.D.H. BHADESHIA**, L. KARLSSON*** and P.J. WITHERS*

**School of Materials, University of Manchester, Grosvenor Street, Manchester M1 7HS, UK*
***Materials Science & Metallurgy, University of Cambridge, Pembroke St, Cambridge, CB2 3QZ, UK*
****ESAB AB, Central Research Laboratories, SE-40277 Gäteborg, Sweden*

ABSTRACT

Weld residual stresses often have serious implications for the integrity of engineering structures. Numerical models provide a way to assess full-field residual stress distributions as a complement to experimental methods. A finite element model was built to estimate the residual stresses that are generated when a single pass weld bead is deposited on to an austenitic stainless steel base plate. The objective was to investigate how and to what extent the martensitic transformation of the stainless steel welding consumable can mitigate potentially harmful tensile residual stresses. Two single-pass welds were deposited using gas metal arc welding (GMAW) on 12 mm thick 304L steel plates using a purpose designed martensitic alloy and a commercial non-transforming austenitic welding alloy. The model was verified with experimental data obtained from neutron diffraction experiments carried out on welded plates.

INTRODUCTION

Residual stress is that which remains in a body after the original cause of the stress (external forces, heat gradient etc.) has been removed. Welding residual stresses [1-2] are major factors in material structural integrity assessments and therefore need to be quantified in engineering design procedures [3-5]. Unfortunately, the non destructive measurement of residual stresses in thick components, such as those that are common in power-plant infrastructure, tends to be both time-consuming and expensive. Furthermore, there are practical limitations associated with many of the available measurement techniques. Taken together these factors have stimulated interest in supplementing measured data with numerical estimates for stress distributions.

Mathematical modelling of welding phenomena is complex involving, for example melt pool phenomena, solidification, heat-flow simulation and electrical-thermal-mechanical simulation effects. In the case of steels, the potential for solid-state phase transformations complicate matters further.

Two common methods of mitigating welding residual stress are post-weld heat treatment and shot peening. An alternative is to design welding filler materials capable of reducing the residual stresses that develop during the welding process [6-8]. This is inspired by the work of Jones and Alberry [9-10], who conducted experiments that illustrate how solid-state phase transformations can compensate stress development in constrained samples of steels. Bainite and martensite are particularly effective in this respect [6-10]. If the transformation exhausts well before cooling is complete, the tensile residual stress can accumulate again due to continued thermal contraction. To mitigate the stress remaining at ambient temperature therefore requires alloys with low transformation temperatures. In view of the large directional shear component associated with the transformation in addition to a dilatation, stress assisted selection of preferred variants could lead to significant directionality of stress relief [6, 8].

A new tough, low-carbon martensitic stainless steel welding alloy, namely, "CamAlloy" (CamAlloy referred to as Alloy2 in Ref. [8]), which is capable of mitigating residuals stresses in the welding of austenitic stainless steel components, has been developed [8] based on a combination of theory and experiments. The martensite-start temperature (M_s) of the new alloy is as low as ~214 ℃ by design. Satoh-type tests [8, 11] suggest that the alloy could lead to a significant reduction in the residual stress in welded plates. The measured mechanical properties, especially toughness, have been designed to be better than commercially used martensitic stainless steel welding filler materials developed for other applications.

The aim of this paper is to assess the performance of the new alloy with respect to residual stress by mathematical modelling and to compare the results against a conventional welding consumable.

EXPERIMENTAL DETAILS

FABRICATION OF WELDS

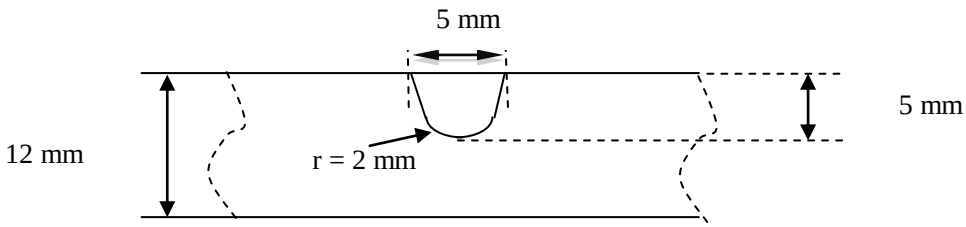

Fig. 1 Details of groove preparation of the welded specimen

Two single-pass welds were deposited using gas metal arc welding (GMAW) on the middle of thick 304L steel plates using the purpose designed martensitic alloy and a commercial non-transforming austenitic welding wire (Table 1). Ambient temperature was ~20 ℃, with no preheat and no clamping during welding.

Each of the base plates had nominal dimensions 300×200×12 mm; the shape of groove preparation for both plates is shown in Fig.1. Alloy, H077 is a low M_s filler with a composition quite similar to CamAlloy. OK Tubrod14.20 is a commercially available austenitic steel. The chemical compositions are listed in Table 1. The welding conditions are summarised in Table 2, weld alloys for plate 1 and plate 2 are H077 and OK Tubrod14.20, respectively.

Table 1 Nominal chemical compositions (wt%) of undiluted filler alloys studied.

Plate Number	**Weld Alloy**	**C**	**Si**	**Mn**	**Ni**	**Cr**	**Mo**	**Cu**	**Fe**
1	H077	0.01	0.8	1.2	6.8	12.5	1.5	0.5	Bal.
2	OK Tubrod 14.20	0.03	0.8	1.2	10.0	19.5			Bal.

Table 2 Summary of welding parameters for each specimen.

Plate Number	Heat Source Power (W)	Welding Speed (mm/s)	Heat Input (kJ/mm)	Current (A)	Voltage (V)
1	7358	7.7	0.96	283	26
2	4224	6.6	0.64	175	24

STRESS MEASUREMENTS IN WELDED PLATES

Neutron diffraction residual stress measurements were made on both welded plates at the SALSA beam line at the Institut Laue-Langevin in France. But only results from plate 1 are presented here as those for plate 2 have not yet been corrected for variations in strain free lattice spacing.

FINITE ELEMENT MODELLING

In the current work, the commercial finite element code SYSWELD [12] was chosen for its capability to model transformation plasticity [13] (Greenwood-Johnson mechanism) although it is realised that this is an approximation given the nature of the deformation associated with displacive transformations. A fully coupled thermo-metallurgical analyses

and a sequentially coupled mechanical analysis were performed. An isotropic hardening model was used to represent strain hardening behaviour for the one-pass welded plate.

Symmetry about the weld centre-line was assumed so that only one half of the geometry was modelled, using 3D linear 8-node brick elements. Two separate models were used for plates 1 and 2 due to difference in the bead profile. The plate 1 model consists of 49200 3D elements, while the plate 2 model 52000 3D elements. A refined mesh was used near the weld and a coarser mesh for the remainder of the plate, as shown in Fig. 2. The structural analysis used the results of the thermal analysis (temperatures) in order to calculate the instantaneous phase mixture and residual stresses.

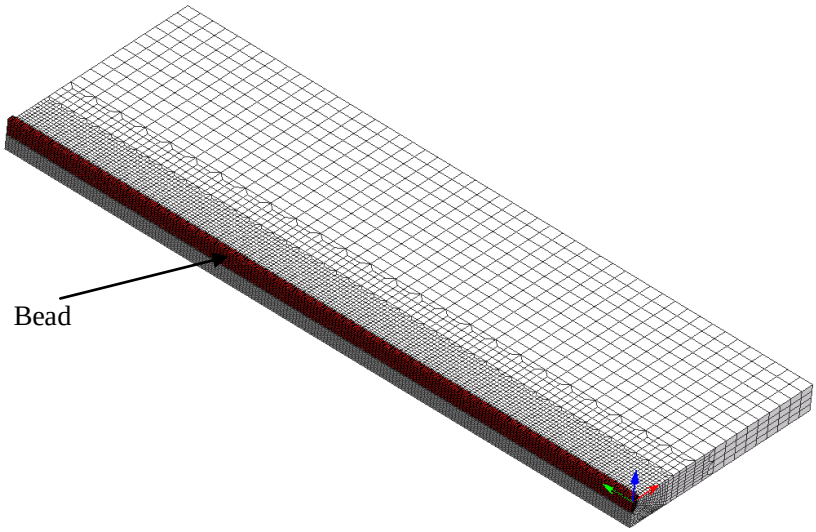

Fig. 2 Mesh for plate 2, with bead highlighted

To model the material deposit during welding, the so-called "chewing gum method" [12] is used instead of conventional element activation. An artificial phase is assigned to the weld beads at the beginning of welding. If heated to a high enough temperature, this phase will transform to austenite, which is an active phase. In this way, the software and the metallurgical model take care of the activation automatically. However, if the heat source intensity is insufficient, the chewing gum material remains as 'chewing gum'. This provides a way to check the thermal model since no chewing gum should remain after welding. Furthermore, this phase has specific material properties, which would have little effect on the stress development of the structure. This method is numerically stable.

MATERIAL PROPERTIES

The welding analysis requires thermo-physical properties such as the specific heat, thermal conductivity, density and coefficient of thermal expansion. In SYSWELD, 2D elements

were used to define the thermal boundary conditions. The heat loss is modelled by a combined convection and radiation coefficient. Mechanical properties such as Young's modulus, Poisson's ratio, yield stress and hardening data are also required. And most of those properties are temperature and phase dependent, particularly the properties of product phases (ferrite, bainite, and martensite) are usually quite different from that of austenite. For instance, the thermal expansion coefficient of austenite is much larger than that of ferrite.

Table 3 Yield stress at room temperature of welding materials and materials actually used in the numerical models

Actual Material	Yield Stress / MPa	Material with full set of properties data available	Yield Stress / MPa
304L	170 (minimum)	304	240
H077	838 (measured)	DP-W-600	840
OK Tubrod 14.20	403 (typical)	Nirost_H400	390

Unfortunately, not all the data were available; some alternative means of obtaining these data was required. Some properties of CamAlloy were used for H077 since they are similar. For example, the tensile properties were assessed by tests for the CamAlloy [8]. The CamAlloy has a yield stress of 840 MPa at room temperature, which compares well with that of 838 MPa with a high strength and dual phase steel available in the SYSWELD literature (DP-W-600). Therefore the DP-W-600 data were used for the alloy.

The properties for the base plate 304L were partly found from literature [14]. They compared well with another closely related austenitic stainless steel 304, which is available in the SYSWELD literature. The 304 data were therefore used for the base plate.

Similarly, data for another austenitic steel Nirost_H400, which is also available in the SYSWELD literature, were used to represent austenitic steel OK Tubrod 14.20 [15]. Table 3 shows the room temperature yield strength used in the models and that actually measured [8] or reported in the literature [14-15].

MARTENSITE TRANSFORMATION

During cooling, the H077 undergoes martensite transformation. The martensite transformation is described by the Koistinen-Marburger [16] relationship.

$$X(T) = 1 - \exp(-b(M_s - T)) \quad \text{for } T < M_s \tag{1}$$

where X is the volume fraction of the transformation product at a given temperature T. There are only two parameters (b and M_s) for this model. Due to current paucity of materials data for H077, those two parameters were taken from a similar alloy, the CamAlloy.

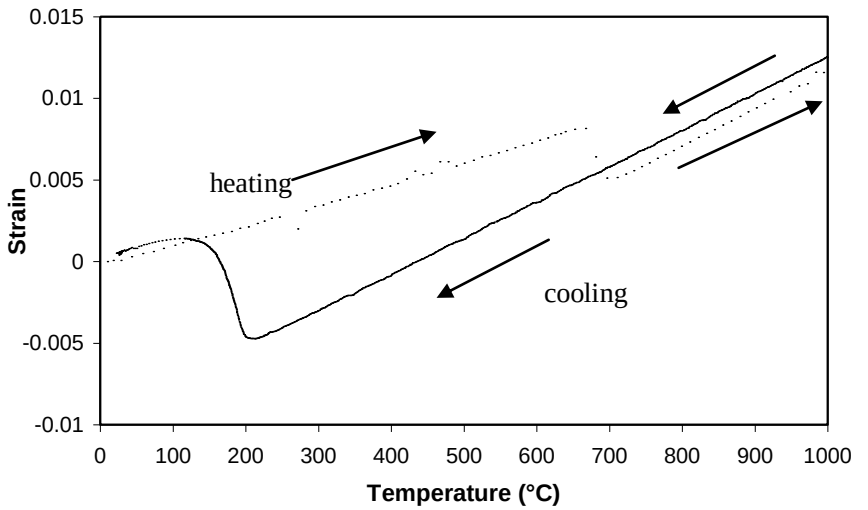

Fig. 3 Dilatometric diagram for a specimen heated and subsequent cooled at 10 ℃/s.

Fig. 3 shows typical results of the dilatometer tests with the M_s temperagure determined to be ~214 ℃ [8]. It also shows that the martensite transformation finishes at about 100 ℃.

In this study, M_s=214 ℃, b=*0.025* were used.

MOVING HEAT SOURCE CALIBRATION

The welding heat input distribution is approximated by the double ellipsoid model based on the work of Goldak [17]. This is a built-in model within SYSWELD and an arc efficiency of 0.75 was assumed throughout this work. The heat power density function is described mathematically by some empirical parameters that need to be calibrated before the heat source can be applied in an analysis. In this work, the calibration was carried out by seeking the best possible reproduction of the fusion zone (FZ) or the heat affected zone (HAZ) in plates 1 and 2.

The FZ/HAZ boundaries are estimated by plotting the maximum temperature envelope (calculated as the maximum temperature at all nodes at any time during the transient) on a contour plot with a maximum contour value of 1400 ℃ and a minimum contour value of 700 ℃. Fig. 4 shows predicted peak temperature contours at the mid-length section perpendicular to the weld bead for plate 1 and 2. They are reasonably close to the outer boundary of the FZ in the macrograph for the plates. It is difficult to match the FZ for plate 1 due to its irregular shape. One of the future studies would be prepare high quality

macrographs showing HAZ more clearly so that more accurate calibration can be carried out by seeking the best reproduction of the HAZ.

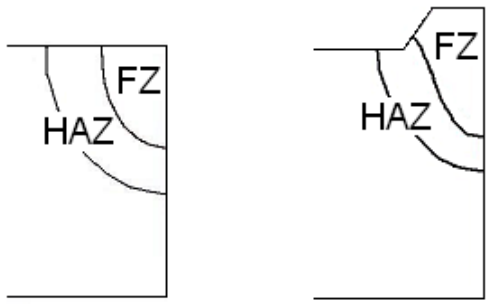

Fig. 4 Predicted 700-1400 ℃ peak temperature plots from mid-length cross section for a) plate 1 and b) plate 2

MECHANICAL ANALYSIS

The components of strain used in the sequential mechanical analyses have been described by Belytschko [18]**.** The total strain rate was partitioned as follows:

$$\dot{\varepsilon} = \dot{\varepsilon}^{e} + \dot{\varepsilon}^{p} + \dot{\varepsilon}^{tp} + \dot{\varepsilon}^{th} \tag{2}$$

where $\dot{\varepsilon}$, $\dot{\varepsilon}^{e}$, $\dot{\varepsilon}^{p}$, $\dot{\varepsilon}^{tp}$, $\dot{\varepsilon}^{th}$ are, respectively, the total, elastic, plastic (or viscoplastic), transformation plasticity, and combined thermal-metallurgical strain rates. The structure of equation (2) is such that the volume-change effects manifest as part of the combined thermal-metallurgical component of strain, while the transformation plasticity term incorporates deformation that arises by the Greenwood-Johnson mechanism. When a multi-phase mixture was present, the composite material properties were estimated according to the following rule of mixtures.

$$\varepsilon^{th}(T) = \sum_{phases} X_i \varepsilon_i^{th}(T) \tag{3}$$

$$\varepsilon_i^{th}(T) = \alpha_i(T)\left[T - T_{ini}\right] \tag{4}$$

where ε_i^{th} is the thermal strain of metallurgical phase *i*. The thermal strain of each phase differs not only by its gradient, representing the coefficient of expansion, but also by its origin ordinate, reflecting a change in volume during transformation. α_i is the expansion coefficient of phase *i*, X_i is the proportion of phase *i*, and T_{ini} is the initial temperature. In this work, expansion coefficients for the ferrite phase and the austenite in welding steel were obtained from the literature.

The phenomenon of transformation plasticity is automatically taken into account (assuming that austenite is the soft phase) by the software. Plastic transformation strain $\dot{\varepsilon}^{tp}$ is computed from the evolution law:

$$\dot{\varepsilon}^{tp} = -\frac{3}{2} Kh(\frac{\sigma_{eq}}{\sigma^y}) S \ln(X_\alpha) \dot{X}_\alpha \tag{5}$$

where *K* is the coefficient of transformation plasticity, X_α is the volume fraction of ferrite, bainite and martensite (phase α), and it is assumed that phase γ is being transformed into phase α, σ_{eq} is the von Mises equivalent stress, σ^y is the yield stress of the phase mixture, *S* the macroscopic homogenized deviator tensor, and *h* a corrector function. In SYSWELD, *K* is computed by the formula proposed by Leblond [13]:

$$K = \frac{2\Delta\varepsilon_{\gamma\to\alpha}^{th}}{\sigma_\gamma^y}$$

with:

$\Delta\varepsilon_{\gamma\to\alpha}^{th}$ difference of thermal strain between phase α and γ

σ_γ^y yield stress of austenite.

RESULTS AND DISCUSSION

The stress results of finite element analyses are shown in Figs. 5-7. In order to understand the predicted effects of transformation dilatation and transformation plasticity on the development of residual stress during cooling, Fig. 5 shows the predicted transient longitudinal stresses as a function of temperature for plate 1 and plate 2, during cooling from ~1200 ℃ to room temperature, at three different points on the weld centreline at the mid-length position of the weld and 0 mm, 1.7 mm, 3.3 mm below the plane of top surface, respectively. All those three points had a peak temperature higher than 1000 ℃ during welding and would be expected to be fully austenitized during heating. The material was set to be annealed at ~1300 ℃. Unsurprisingly, for all the modelling cases, almost zero stress or compressive stress (if peak temperature is less than annealing temperature) exists at a

temperature higher than 1000 ℃. Tensile stresses then begin to develop on cooling from 1000 ℃ due to thermal contraction but limited by elevated temperature yield strength. The residual stress within the conventional austenitic weld alloy OK 14.20, for which no phase transformation is considered in the model, accumulated continuously until room temperature was reached. In contrast, in the H077 alloy, the tensile stress relieved because of expansion caused by martensitic transformation, and compressive stress develops until the transformation is almost exhausted (~100 ℃). After that, presumably the thermal contraction became dominant again and the compressive stress is reduced. Perhaps surprisingly, the reduction of the compressive stress is so small for all the three points that none of them attain tensile stress state at room temperature. Only the point at the top surface (i.e., 0 mm below) in the H077 exhibits a stress close to zero, the other two points exhibit substantial compressive stress. Nevertheless, this clearly demonstrates that the martensitic transformation in the new weld alloys leads to a potentially less harmful stress distribution in and near the fusion zone.

Figs. 6-7 show the predicted results for plate 1 and 2, as well as the neutron diffraction measurement result for plate 1. In Fig.6, each of the contour plots shows the longitudinal stresses that were predicted or measured over the mid-length cross section of the weld. All the measurement points are marked with crosses in the stress maps. It can be seen that no measurements were made at both top and bottom surfaces. The stresses at depths less than 2 mm or greater than 10 mm were estimated by extrapolations for the first stress map. Symmetry was assumed about the weld centreline in the experimental calculations, with each calculated stress averaged with the value at the corresponding mirror image location about the weld centreline. Thus the results plotted in the first stress map of Fig. 6 correspond to averaged values.

In the FZ/HAZ of plate 1, both prediction and measurement show that the martensitic transformation has resulted in a low level tensile or compressive stress. Tensile stress increases below the HAZ along the weld centreline until reaching a peak stress. In contrast, in the weld made with the conventional non transforming austenitic steel, high tensile stress arises in the FZ reaching a peak at a depth of 4mm. This is the major difference between plate 1 and plate 2.

Differences are also evident for the predictions and the measurements. The measurement of plate 1 shows a peak tensile stress of about 600 MPa located about 8 mm below the top surface. This might suggest that strong hardening behaviour exists for the base plate. It could be due to the differences between current material properties used in the model and the actual material properties of the welded 304L plate. And in the model, M_s for CamAlloy was used. But dilution with the base metal would change the weld metal composition and increase M_s significantly, which will affect calculated stresses.

In the transverse direction, the predictions show more localised behaviour than the measurements. In both models, compressive stresses are dominant 20 mm beyond the weld centreline, in contrast, low tensile stress are evident until 30 mm away from the weld centreline.

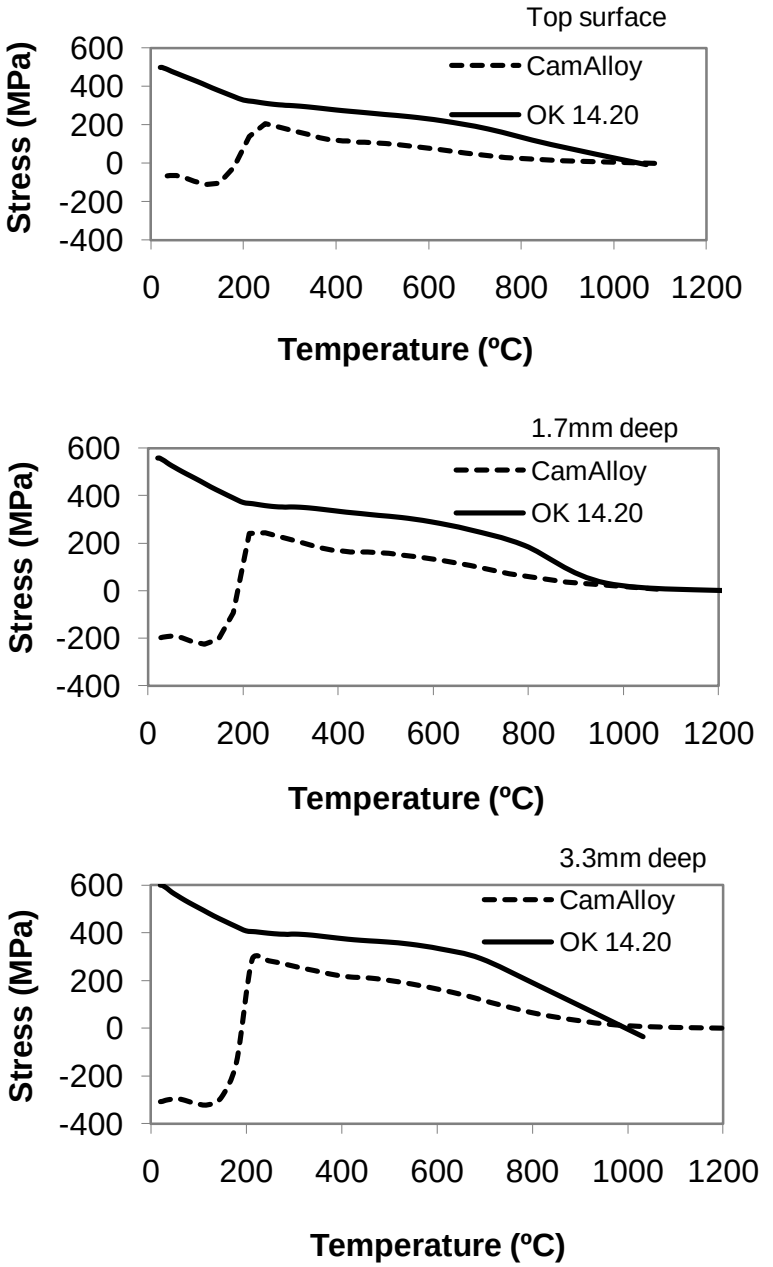

Fig. 5 Predicted transient longitudinal residual stress for plate 1 and 2 plotted against temperature during cooling at mid-length position of weld, on weld centreline, and at different depths within each welded plate

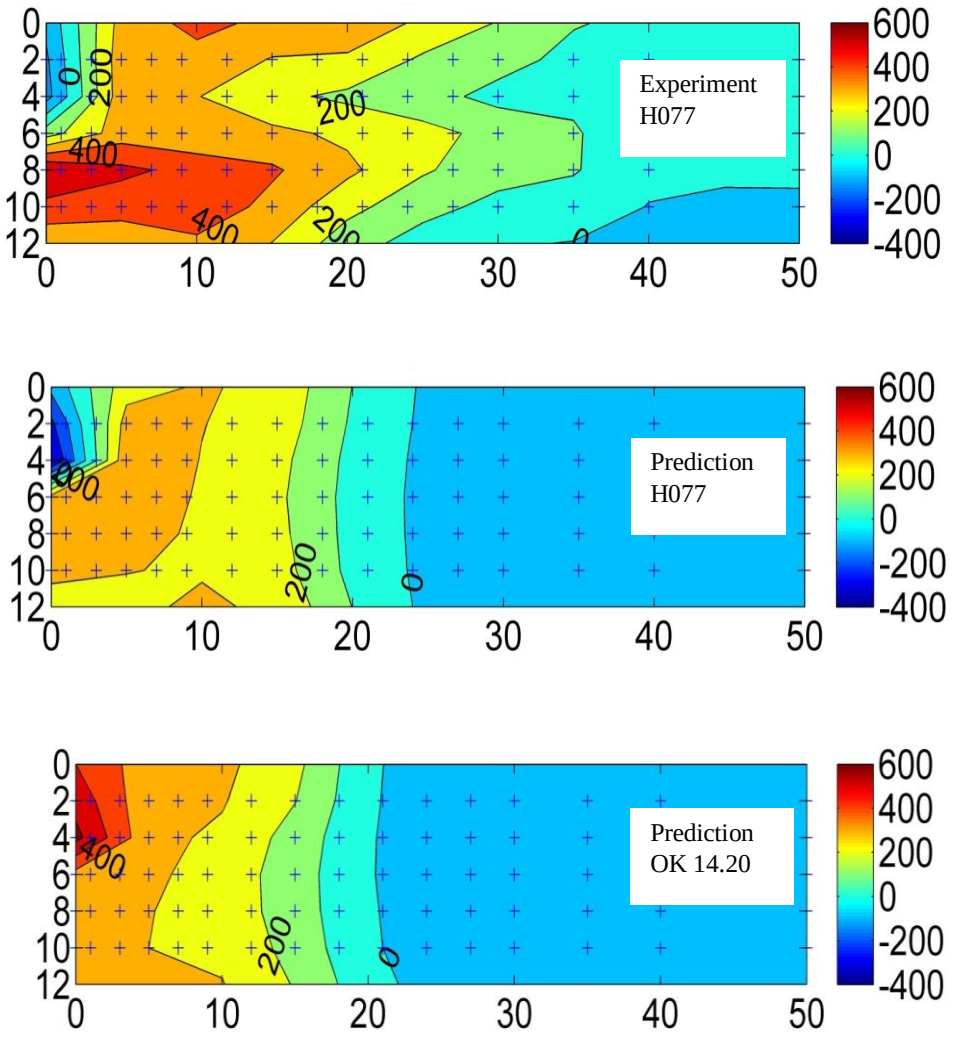

Fig. 6 Residual stress contours (in MPa) for longitudinal orientations as measured over the mid length cross-section (in mm) by neutron diffraction for plate 1 and as predicted for plates 1 and 2, with crosses marking the measurement positions.

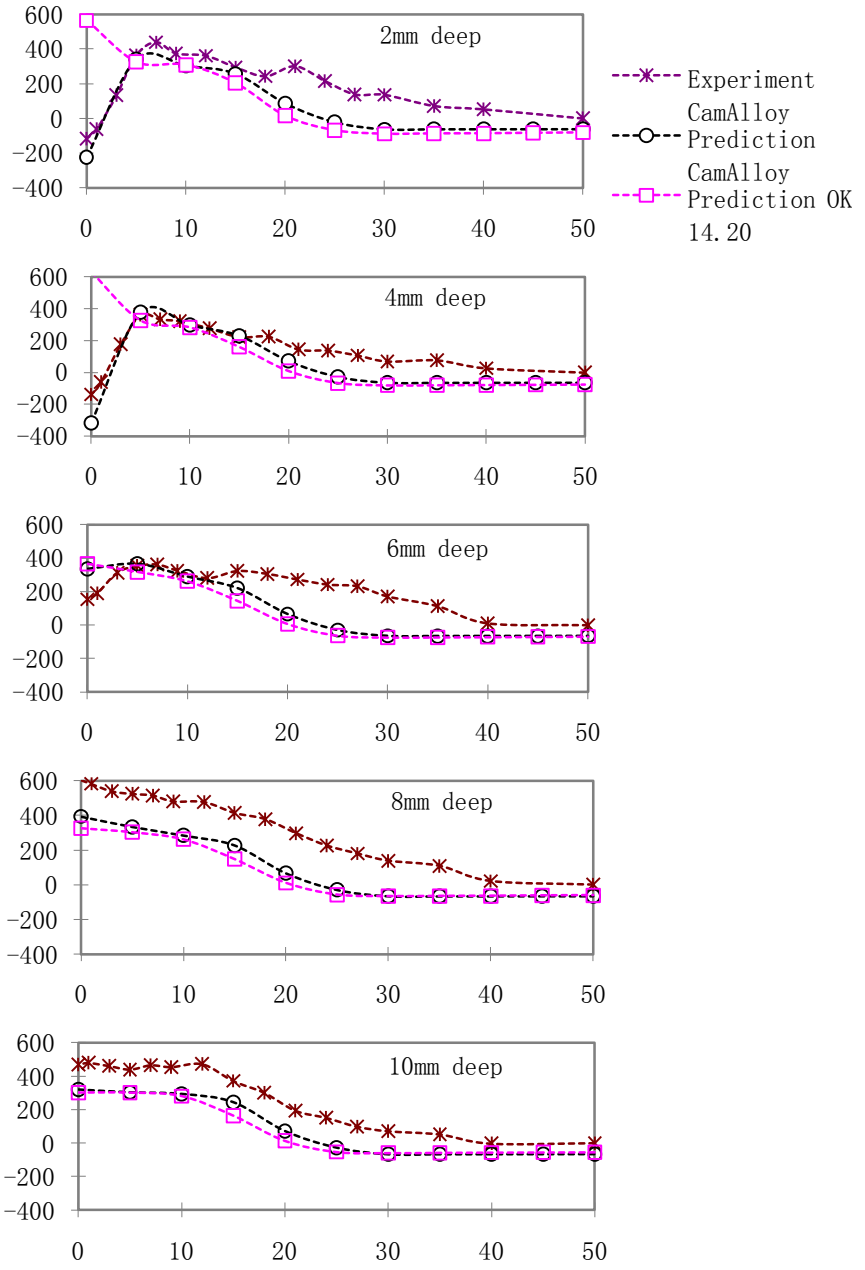

Fig. 7 Variation in longitudinal residual stress (in MPa) as predicted with distance (in mm) from weld centreline at different depth within each welded plate, and as measured for plate 1

The variation in longitudinal residual stress with distance from weld centreline is shown again for each case in Fig. 7. Here each plot corresponds to a different depth below the top surface of the welded plate. The extent to which compressive stresses are induced within the weld FZ by the martensitic transformation is obvious in the first 2 plots, which correspond to depths of 2 and 4 mm respectively. The prediction and measurement show good agreement within the FZ in those two plots.

Immediately under the FZ and close to the weld centreline, at a depth of 6 mm, the prediction show higher tensile stresses than measured. While at a depth of 8 mm, where the experimental residual stress peaks, there is a clear displacement between the measured and the predicted stress curve, with the former about 200 MPa higher. The same trend is evident at a depth of 10 mm, with a smaller displacement between the prediction and measurement.

The side by side comparison of the two models illustrates the effect of the phase transformation in the weld filler since the same baseplate properties were used in each case. Considering residual stress level at all the depths, the results from the two numerical models show that martensitic transformation can effectively mitigate residual tensile stress at ambient temperature. The neutron measurements show that the transformation also reduces the tensile stress in the HAZ.

CONCLUSIONS

Two finite element analyses have been carried out on single-pass welds, which were deposited by using gas metal arc welding (GMAW) on 12 mm thick 304L steel plates using a purpose designed martensitic alloy and a commercial non-transforming austenitic welding alloy. It has been shown that the martensitic transformation of weld alloy with a low M_s can significantly reduce the build up of tensile stress within the HAZ during cooling. This also shows that phase transformation has significant effects on the predicted residual stresses in transforming materials and therefore should be accounted for.

The model was verified using the experimental data obtained from neutron diffraction, carried out on the welded plate 1. The numerical results compare quite well with experimental results within the HAZ, while less agreement achieved outside the HAZ. It is possible that the discrepancies between the prediction and the measurement outside the HAZ could be improved if the actual material properties were used in the model. It should also be noted that the weld model used includes only the dilatational component of the transformation. It is possible that preferred orientation could lead to significant directional variations in the transformation strain. This will be the topic of further studies. More accurate calibration of the thermal model would help the verification as well.

ACKNOWLEDGEMENTS

HD and AFM would like to acknowledge support from Rolls-Royce Marine. HD would like to thank Dr M. Keavey at the University of Manchester for thoughtful discussions.

REFERENCES

[1] J.A. Francis, H.K.D.H. Bhadeshia, and P.J. Withers: "Welding Residual Stresses in Ferritic Power-Plant Steels", *Mat. Sci. Tech.*, 2007, **23** (9), 1009-20.

[2] P.J. Withers: "Residual Stress & its Role in Failure", Rep. Prog. Phys., 2007, **70**, 2211-2264.

[3] D.P.G. Lidbury: "The Significance of Residual Stresses in Relation to the Integrity of LWR Pressure Vessels", *International Journal of Pressure Vessels and Piping*, **17** (4), 197-328, 1984.

[4] R.A. Ainsworth, The Treatment of Thermal and Residual-Stresses in Fracture Assessments. Engineering Fracture Mechanics, 1986. **24**(1): p. 65-76.

[5] A. Stacey, J.Y. Barthelemy, R.H. Leggatt, and R.A. Ainsworth, Incorporation of residual stresses into the SINTAP defect assessment procedure. Engineering Fracture Mechanics, 2000. **67**(6), 573-611.

[6] J. A. Francis, H. J. Stone, S. Kundu, R. B. Rogge, H. K. D. H. Bhadeshia, P. J. Withers, and L. Karlsson. Transformation temperatures and welding residual stresses in ferritic steels. In Proceedings of PVP2007, ASME Pressure Vessels and Piping Division Conference, pages 1–8, San Antonio, Texas, 2007. American Society of Mechanical Engineers, ASME.

[7] H. Dai, J. A. Francis, H. J. Stone, H. K. D. H. Bhadeshia, and P. J. Withers. Characterising phase transformations and their effects on ferritic weld residual stresses with X–rays and neutrons. Metallurgical & Materials Transactions A, 39:3070–3078, 2008.

[8] A.A. Shirzadi, H.K.D.H. Bhadeshia, L. Karlsson and P.J. Withers: "Stainless steel weld metal designed to mitigate residual stresses", *Science and Technology of Welding and Joining*, **14** (6), 559-565, 2009.

[9] W.K.C. JONES and P.J. ALBERRY: in "Ferritic Steels for Fast Reactor Steam Generators", 1-4, London, British Nuclear Engineering Society, 1977.

[10] W.K.C. JONES and P.J. ALBERRY: in "Residual Stresses in Welded Constructions", The Welding Institute, Cambridge, 1977.

[11] K. Satoh: "Transient Thermal Stresses of Weld Heat-Affected Zone by Both-Ends-Fixed Bar Analogy", Trans. of the Japan Welding Soc., **3**, 125-134, 1972.

[12] ESI Group, 2007, SYSWELD, Theory Manuals, ESI UK, John Eccles House, the Oxford Science Park, Oxford.

[13] Leblond J.B., Mottet G. & Devaux J.C., "A theoretical and numerical approach to the plastic behaviour of steels during phase transformation, I : Derivation of general relations, II : Study of classical plasticity for ideal-plastic phases", Jour. of the Mech. and Phys. of Solids, **34** (4), 395-432, 1986.

[14] http://www.azom.com/Details.asp?ArticleID=965

[15] http://pdf.directindustry.com/pdf/esab/welding-consumables-handbook/18224-100778-_243.html

[16] D. P. Koistinen and R. E. Marburger, Acta Metallurgica, 7, p59-60, 1959.

[17] J. Goldak, A. Chakravarti and M. Bibby: "A New Finite-Element Model for Welding Heat-Sources", Metallurgical Transactions B – Process Metallurgy, **15** (2), 299-305, 1984.

[18] Belytschko, W. K. Liu and B. Moran, Nonlinear Finite Elements for Continua and Structures, John Wiley & Sons, Chichester, 2000.